

We are IntechOpen, the world's leading publisher of Open Access books Built by scientists, for scientists

4,800

Open access books available

122,000

International authors and editors

135M

Downloads

Our authors are among the

154

Countries delivered to

TOP 1%

most cited scientists

12.2%

Contributors from top 500 universities



WEB OF SCIENCE™

Selection of our books indexed in the Book Citation Index
in Web of Science™ Core Collection (BKCI)

Interested in publishing with us?
Contact book.department@intechopen.com

Numbers displayed above are based on latest data collected.

For more information visit www.intechopen.com



Preparation of Nanocellulose with Cation-Exchange Resin Catalysed Hydrolysis

Huang Biao, Tang Li-rong, Dai Da-song,
Ou Wen, Li Tao and Chen Xue-rong
*Fujian Agriculture and Forestry University,
China*

1. Introduction

Cellulose is the most abundant organic compound on earth and is present in a wide variety of living species, such as animals, plants and bacterial (Tingaut et al., 2010; Elazzouzi-Hafraoui et al., 2008). This linear polymer is constituted of repeating β -D-glucopyranosyl units joined by 1 \rightarrow 4-glycosidic linkages. The molecules of cellulose are stabilized laterally by hydrogen bonds between hydroxyl groups and oxygens of adjacent molecules. However, they can be broken chemically under strong aqueous acid or high temperature. Manipulating cellulose molecules on the nanometer scale to create the nanocellulose of excellent properties has become a hotspot of cellulose science. As for nanocellulose, it is currently believed that at least one of its dimension is lower than 100nm. Moreover, nanocellulose exhibits the property of certain gels or fluids under normal conditions. Compared with microcrystalline cellulose, nanocellulose presents very attractive properties such as low density, high chemical reactivity, high strength and modulus, and high transparency (Nogi et al., 2009; Lee et al., 2008; Pääkko et al., 2007; Siró & Plackett, 2001). Therefore, nanocellulose has a great potential for use as filler in nanocomposites and have attracted a great deal of interest recently. Nanocellulose has been reported to improve the mechanical properties by incorporating into a wide range of polymer matrices, including poly(3-hydroxybutyrate), hydroxypropyl cellulose, poly(L-lactide), waterborne polyurethane, poly(3,4-ethylenedioxythiophene), polyvinyl acetate, poly(o-ethoxyaniline). The composite applications may be for use as coatings and films, paints, foams, packaging. (Cai et al., 2011; Zimmermann et al., 2010; Pei et al., 2010; Wang et al., 2010; Mendez & Weder, 2010; de Rodriguez et al., 2006; Medeiros et al., 2008). Moreover, the potential of nanocellulose applications in the area of paper and paperboard manufacture is obvious. Nanocellulose are expected to enhance the fiber-fiber bond strength and, hence, have a strong reinforcement effect on paper materials. Nanocellulose may be useful as a barrier in grease-proof type of papers and as a wet-end additive to enhance retention, dry and wet strength in commodity type of paper and board products. Nanocellulose also can be used as a low calorie replacement for today's carbohydrate additives used as thickeners, flavour carriers and suspension stabilizers in a wide variety of food products and is useful for producing fillings, crushes, chips, wafers, soups, gravies, puddings etc. On the other hand, the food applications were early recognised as a highly interesting application field for nanocellulose due to the rheological behaviour of the nanocellulose gel (Wikipedia, 2011).

The preparation of nanocellulose derived from wood was introduced more than two decades ago (Aulin et al., 2009). Although wood is one of the main resources for the cellulose, competition from different sectors such as the building products and furniture industries and the pulp and paper industry, as well as the combustion of wood for energy, makes it challenging to supply all users with the quantities of wood needed at reasonable cost (Siró & Plackett, 2001). Besides wood, nanocellulose also could be prepared from many agricultural residue and crops, such as cotton, hemp, sisal, bagasse, wheat straw. Therefore, nanocellulose will be key to the development of higher-value agricultural residue products and could find economic interest (de Mesquita et al., 2010). In literature, there are many reports on nanocellulose prepared from diverse non-wood sources including wheat straw (Panthapulakkal et al., 2006; Kaushik et al., 2010; Alemdar & Sain, 2008), potato tuber cells (Dufresne et al., 2000), sisal (Morán et al., 2008; de Rodriguez et al., 2006) and banana rachis (Zuluaga et al., 2009).

Sulfuric acid hydrolysis of cellulose is a well-known process to remove amorphous regions, leaving the crystalline segments intact and leading to the formation of high purity single crystals (de Mesquita et al., 2010). Ion-exchange resins have been used commercially as solid acid catalysts in many areas, such as alkylation with olefins, alkyl halides, alkyl esters, isomerization, transalkylation and nitration. Compared with liquid acid, the main advantages of cation-exchange resin include reduced equipment corrosion, ease of product separation, less potential contamination in waste streams and recycle of the catalyst (Harmer & Sun, 2001).

Moreover, the energy of ultrasound is transferred to the polymer chains through a process called cavitation, which is the formation, growth, and violent collapse of cavities in the water. The energy provided by cavitation in this so-called sonochemistry is approximately 10-100kJ/mol, which is within the hydrogen bond energy scale (Tischer et al., 2010). It can accelerate hydrogen ions to penetrate into the cellulose amorphous chains, promoting the hydrolytic cleavage of the glycosidic bonds (Zhao & Feng, 2007; Filson & Dawson-Andoh, 2009; Wang & Cheng, 2009).

In this study, we aim to present an environmentally and economically novel way to prepare nanocellulose from microcrystalline cellulose by using cation-exchange resin as catalyst with ultrasonic-assisted hydrolysis. Response surface methodology and Box-behnken statistical experiment design method were employed for modeling and optimization of the influence of operating variables on the yield of nanocellulose. In addition, the characterization for morphologies, structure, spectrum properties and rheological behaviors of nanocellulose were also investigated.

2. Experimental section

2.1 Materials

Microcrystalline Cellulose (MCC) used in the experiment was purchased from Shandong Ruitai Chemicals Co., Ltd. The catalyst, NKC-9 cation-exchange resin (NKC-9), was provided by the Chemical Plant of Nankai University of China. It is a macroreticular copolymer styrene-divinyl benzene in H⁺ form and has the following properties: exchange capacity (mmol/g [H⁺]) ≥ 4.7, pearl size of 0.45-1.25 mm, true wet density of 1.20-1.30 g/mL. The resin was firstly pretreated by distilled water to eliminate some impurities and then dried in an oven at 50 °C for 24 h. Dried resin was used for further experimental studies.

2.2 Sample preparation

Nanocellulose was isolated from MCC by means of cation-exchange resin hydrolysis. 3 g dried MCC and 30 g ion exchange resin were put into 250 ml distilled deionized water. The suspension was stirred and sonicated at 40-60°C for 150-210min. Then the ion exchange resin was separated from cellulose suspension. The resulting suspension was centrifuged several times at 12000 rpm and washed with distilled deionized water until the supernatant became turbid, and then the nanocellulose was collected.

2.3 Experimental design and statistical analysis

The Box-Behnken experimental design method was used to determine the effects of major operating variables on the yield of nanocellulose and to find the combination of variables in order to produce maximum nanocellulose yields. The advantage of Box-Behnken design is that it has only three levels, coded -1, 0, and +1 for low, middle and high concentrations, respectively. This experimental design reduced the number of experiments, so it is more efficient and easier to arrange and to interpret in comparison to others (Majumder et al., 2009). Therefore, this statistical technique was adopted in this study.

The experiments at ratio of NKC-9 to MCC (5: 1, 10: 1 and 15: 1), temperature (40, 50 and 60°C), time (150, 180 and 210min) were employed simultaneously covering the spectrum of variables for the percentage of nanocellulose yield in the Box-Behnken Design. As presented in Table 1, the experimental design involved three parameters (X_1 , X_2 and X_3), each at three levels, coded -1, 0, and +1 for low, middle and high concentrations, respectively. A second-order polynomial equation was used to express the responses as a function of the independent variables as follows:

$$Y = B_0 + \sum_{i=1}^n B_i X_i + \sum_{i=j=1}^n B_{ij} X_i X_j \quad (1)$$

Where Y represents the measured response variables, three variables are involved and hence n takes the value 3. B_0 is the constant coefficient, B_i s are the linear coefficients, B_{ij} s are the interaction coefficients.

Factor	Symbols & level ^b		
	-1	0	+1
ratio of resin X_1	5	10	15
temperature X_2 (°C)	40	50	60
time X_3 (min)	150	180	210

^b $x_1=(X_1-10)/5$; $x_2=(X_2-50)/10$; $x_3=(X_3-180)/30$.

Table 1. Code and level of factors chosen for the trials.

2.4 Characterization of nanocellulose

Electron microscopy was conducted to observe the surface of MCC and nanocellulose. Samples were mounted on metal stubs by double side adhesive tape and examined with FEI XL30 ESEM-FEG field emission scanning electron microscopy (FESEM). The nanostructure of nanocellulose was examined in a transmission electron microscope (TEM), Tecnai G2F20 FETEM (FEI Co. Ltd., USA) at an acceleration voltage of 200 kV. The X-ray diffraction

(XRD) patterns were recorded by a X'Pert Pro MPD X-ray diffractometer equipped with Cu K α radiation ($\lambda = 0.154$ nm). Fourier transform infrared spectroscopy (FTIR) was used to examine any changes in the chemical structure of samples. A Nicolet 380 (Thermo electron Instruments Co., Ltd., USA) was used to obtain the spectra of each sample. The rheological behavior of sample was examined by DV-III+pro rheometer (Brookfield Engineering Laboratories, Inc., USA) with SC4-34 spindle.

3. Results and discussion

3.1 Optimization of hydrolysis conditions for nanocellulose

The effect of process variables like ratio of NKC-9 to MCC, temperature and time on the preparation of nanocellulose was investigated by means of response surface methodology, Box-Behnken Design (BBD). Table 2. shows the coded value of the variables and the yield of nanocellulose (response). The whole design consisted of 17 experimental points carried out in random order. Five replicates at the centre of the design were used to estimate a pure error sum of squares. The data obtained was analyzed by applying multiple regression analysis method based on Eq. (1). The predicted response Y for nanocellulose yield was obtained and shown as:

$$Y = 50.68 + 0.15X_1 - 1.11X_2 + 1.67 X_3 + 0.74X_1 X_2 - 0.35X_1 X_3 - 1.07X_2 X_3 - 3.85X_1^2 - 3.83X_2^2 - 5.17 X_3^2 \quad (2)$$

In this equation, Y is the predicted response variable, i.e., the yield of nanocellulose (%), X_1 , X_2 and X_3 are the independent variables in coded units, i.e., ratio of NKC-9 to MCC, temperature and time, respectively.

The data obtained from Eq. (2) are significant. It is verified by F-value and the analysis of variance (ANOVA) by fitting the data of all independent observations in response surface quadratic model. The summary of the analysis of variance (ANOVA) of the results of the quadratic model fitting are shown in Table 3. ANOVA is indispensable to testing the significance and adequacy of the model. The corresponding variables would be more significant if the absolute F-value becomes greater and the p-value becomes smaller (Chen et al., 2010). The model F-value of 42.80 implies that the model is significant. There is only a 0.01% chance that a "model F-value" this large could occur due to noise. Value of "Prob > F" less than 0.05 indicates that the model terms are significant. In this case, X_2 , X_3 , X_2X_3 , X_1^2 , X_2^2 and X_3^2 are significant model terms. However, ratio of NKC-9 to MCC (X_1) and interaction terms (X_1X_2 and X_1X_3) had a negative effect on Y.

The "Lack of fit F-value" of 4.79 implies that the lack of fit is not significant relative to the pure error. There is a 8.23% chance that a "Lack of fit F-value" this large could occur due to noise. The determination coefficient (R^2), a measure of the goodness of fit of the model, was very significant at the level of 98.22%, the model was unable to explain only 1.78% of the total variations. The value of adjusted R^2 , was also very high at the level of 0.9592, indicating high significance of the model.

The effect of hydrolysis conditions on the yield of nanocellulose is shown in Table 2 by the coefficient of the second-order polynomials. To visualize and identify the type of interactions between test variables, the two and three dimensional contour plots are shown in Fig. 1, including ratio of NKC-9 to MCC and temperature, ratio of NKC-9 to MCC and time, as well as temperature and time. The circular contour plots indicate that the interaction

Trial No.	X_1	X_2 (°C)	X_3 (min)	Yield of NCC, Y (%)	
				Experimental	Predicted
1	0(10)	0(50)	0(180)	50.38	50.68
2	0(10)	-1(40)	1(210)	45.86	45.54
3	-1(5)	-1(40)	0(180)	43.71	44.71
4	0(10)	0(50)	0(180)	50.63	50.68
5	0(10)	-1(40)	-1(150)	40.79	40.05
6	0(10)	0(50)	0(180)	51.64	50.68
7	0(10)	0(50)	0(180)	50.38	50.68
8	0(10)	0(50)	0(180)	50.38	50.68
9	1(15)	-1(40)	0(180)	43.46	43.52
10	-1(5)	0(50)	1(210)	44.22	43.54
11	1(15)	0(50)	-1(150)	39.82	40.49
12	1(15)	0(50)	1(210)	42.88	43.13
13	-1(5)	1(60)	0(180)	41.07	41.01
14	1(15)	1(60)	0(180)	43.77	42.78
15	0(10)	1(60)	-1(150)	39.66	39.98
16	-1(5)	0(50)	-1(150)	39.76	39.50
17	0(10)	1(60)	1(210)	40.43	41.17

Table 2. Experimental designs and results.

between the corresponding variables is negligible. An elliptical or saddle nature of the contour plots indicates significance of the interactions between the corresponding (Majumder et al., 2009; Fu et al., 2007).

As can be seen in the plots, the two and three dimensional contour plots with NKC-9 to MCC and temperature had a circular nature, indicating a negligible interactive effect on the yield between the two independent variables (Fig.1A). The yield of nanocellulose increased with rise in ratio of NKC-9 to MCC and temperature.

Factors	SS ^a	DF ^b	MS ^c	F-Value	Prob.(P)>F
Model	303.22	9	33.69	42.80	<0.0001
X_1	0.17	1	0.17	0.22	0.6559
X_2	9.88	1	9.88	12.55	0.0094
X_3	22.34	1	22.34	28.38	0.0011
X_1X_2	2.19	1	2.19	2.78	0.1395
X_1X_3	0.49	1	0.49	0.62	0.4559
X_2X_3	4.62	1	4.62	5.87	0.0459
X_1^2	62.36	1	62.36	79.21	<0.0001
X_2^2	61.81	1	61.81	78.52	<0.0001
X_3^2	112.36	1	112.36	142.73	<0.0001
Residual	5.51	7	0.79		
Lack of Fit	4.31	3	1.44	4.79	0.0823
Pure Error	1.20	4	0.30		
Total	308.73	16			

^aSS, Sum of Squares. ^bDF, Degrees of Freedom. ^cMS, Mean Square.

Table 3. Analysis of variance (ANOVA) for the the yield of nanocellulose.

As shown in Fig.1, in the design boundary, each response surface plot had a clear peak and the corresponding contour plot had a clear maximum, which means that the maximum hydrogen yield could be achieved inside the design boundaries (Ghosh & Hallenbeck, 2010). The yield of nanocellulose increased with increasing ratio of NKC-9 to MCC, temperature and time to the optimal levels, and then decreased with a further increase in these parameters. The optimized conditions for maximum nanocellulose yield can be obtained by Design-expert software. The optimum values of the test variables in uncoded units obtained were ratio of NKC-9 to MCC 9.97: 1, temperature 48.30°C, time 189.00min. At these optimized conditions, the model predicted that the maximum yield of nanocellulose is 50.93%.

As to the actual experimental condition, some conditions were modified as follows: ratio of NKC-9 to MCC 10: 1, temperature 48°C and time 189min. To confirm the model adequacy for predicting maximum yield, three replicates experiments under modified conditions were conducted and the maximum yield of nanocellulose obtained was 50.04% which agreed well with the predicted value.

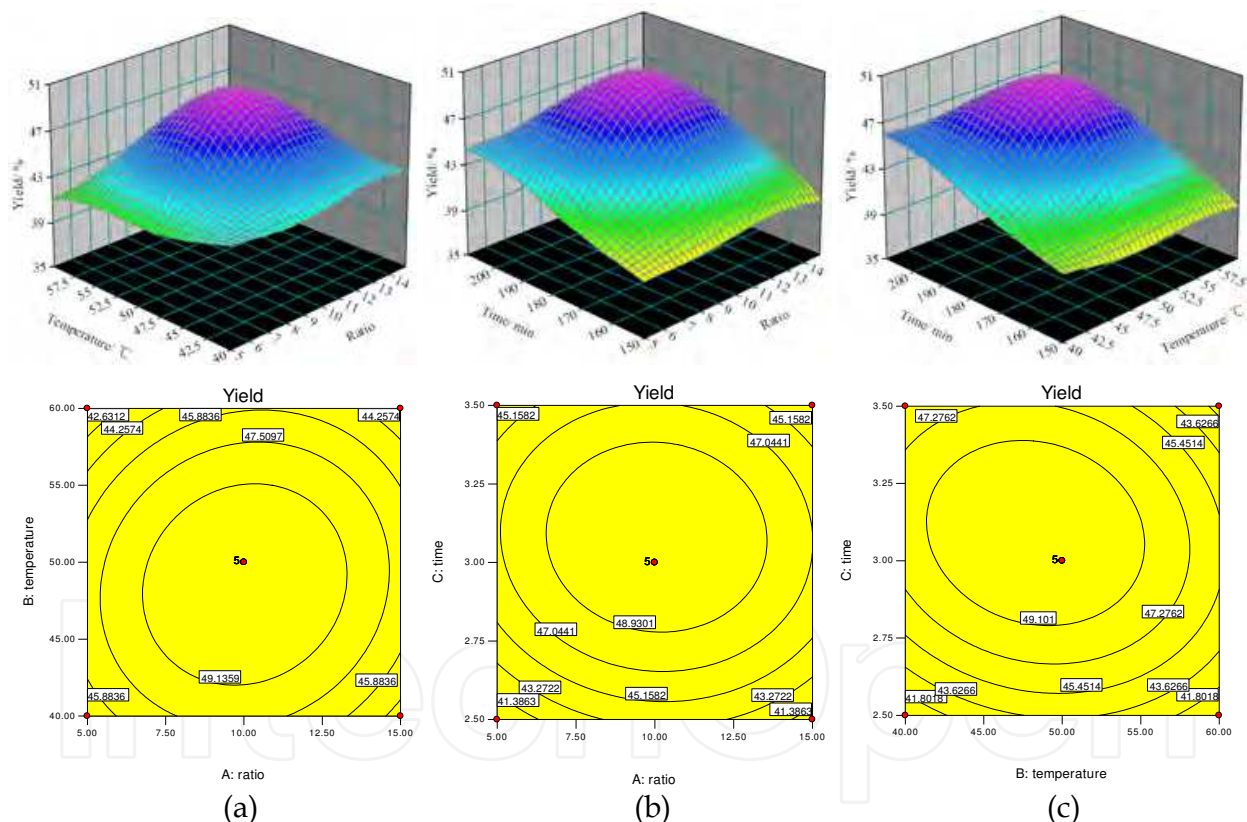


Fig. 1. Two and three dimensional contour plots for the maximum yield of nanocellulose. RSM plots were generated with the data shown in Table 2. (a) Yield of nanocellulose (%) as a function of ratio of NKC-9 to MCC and temperature. (b) Yield of nanocellulose (%) as a function of ratio of NKC-9 to MCC and time. (c) Yield of nanocellulose (%) as a function of temperature and time.

The interactions between ratio of NKC-9 to MCC and time are not perfectly elliptical (Fig.1(b)). The yield of nanocellulose increased with time rising up to certain level, beyond which yield declined slightly. This may be due to that over reaction time completely digests

the cellulose so as to yield its component sugar molecules. Fig.1(c) shows the effect of temperature and time on the yield of nanocellulose. The result had an elliptical nature, indicating a significant interactive effect of the two independent variables on the yield.

3.2 Morphology of microcrystalline cellulose and nanocellulose

Fig.2 shows the morphologies of NCC at different concentrations. After hydrolysis and centrifugation process, the NCC with the concentration of 1% is obtained as shown in Fig.2(a). The micrograph of NCC in Fig.2(b) presents the glossy hydrogel at the concentration of 9%. The appearance of a stable gel is an obvious indication of the presence of NCC. The NCC powder is obtained by freeze drying (Fig.2(c)). It exhibits white metallic luster colour. As is shown in Fig.2(d), evaporation of aqueous suspensions of NCC at room temperature produces solid films with perfect optical transparency.



Fig. 2. Macrostructure of NCC.

Figure.3 compares the morphology of MCC (cf. Fig.3(a)) and NCC (cf. Fig.3(b) and Fig.3(c)). The diameter of MCC is around $15\mu\text{m}$, the length is about $20\text{-}80\mu\text{m}$. After treatment, a remarkable outcome of this novel nanocellulose extraction method can be seen in Fig.3(b) and Fig.3(c). This image also shows that nanocellulose with uniform diameter of approximately $2\text{-}24\text{ nm}$ can be obtained after hydrolysis, and these nanocellulose can form a very fine network. The diameter distribution of nanocellulose was determined with FEG-TEM (cf. Fig.3(c)), and the result is plotted in the following figures.

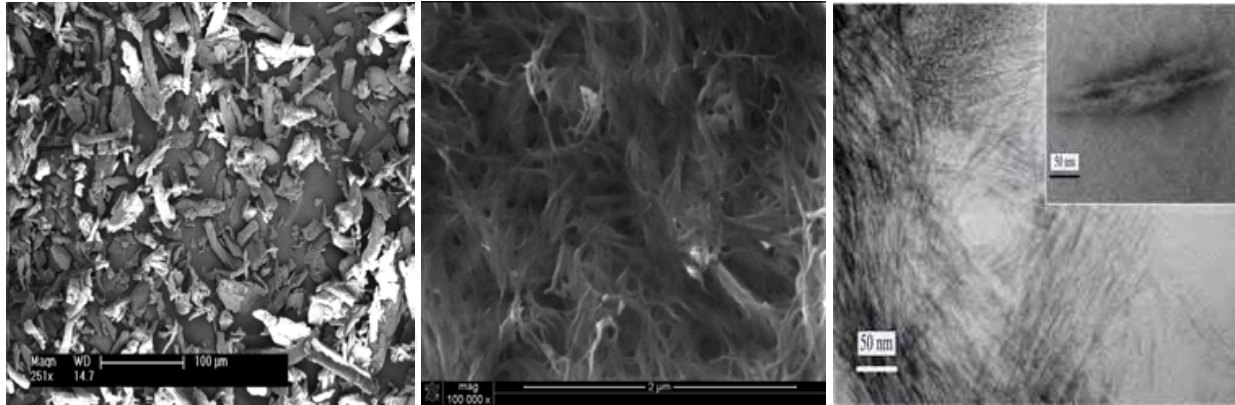


Fig. 3. Morphology of (a) MCC (by FEG-SEM, x 251); (b) NCC (by FEG-SEM, x 100 00) and (c) NCC (by FEG-TEM).

3.3 X-ray diffraction analysis

X-ray crystallography was used to compare the crystallinity of MCC and NCC. Results of X-ray powder diffraction photograph from MCC and NCC are shown in Fig.4(a) and 4(b), respectively. Fig.4 shows that the major crystalline peak which represents the cellulose crystallographic plane (002, Bragg reflection) occurs at $2\theta = 22.667^\circ$ and $2\theta = 22.521^\circ$ for MCC and NCC, respectively. Compared with MCC (crystallinity 75.2%), after cation-exchange resin catalytic hydrolysis, the crystallinity of nanocellulose is 84.26%. The increase in crystallinity may be due to the removal of amorphous regions in the cellulose. This leads to the realignment of cellulose molecules. This also indicates that the nanocellulose obtained by this novel isolation may be more effective in achieving higher reinforcement for composite materials.

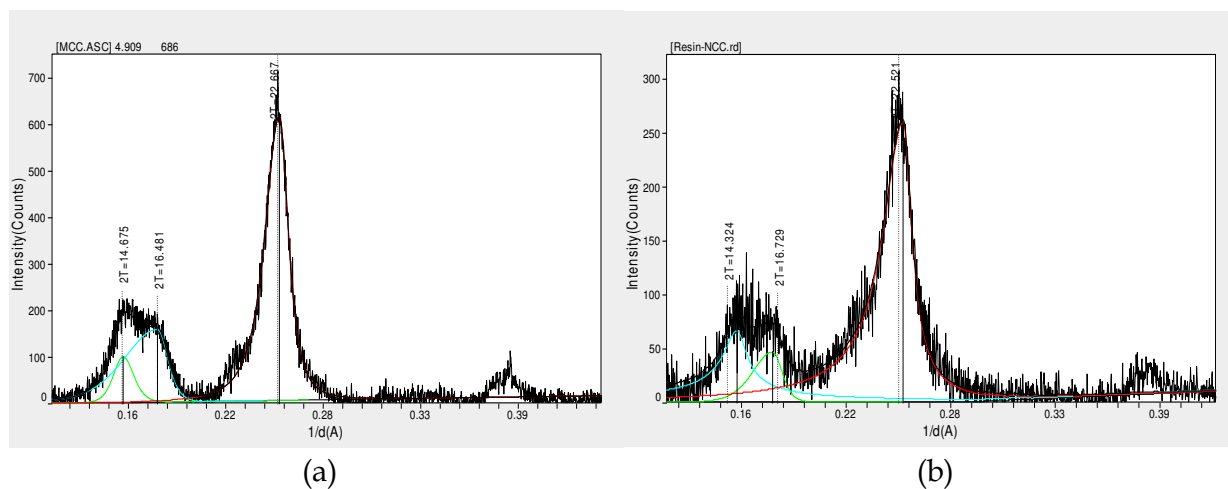


Fig. 4. XRD patterns of (a) NCC and (b) MCC.

3.4 FTIR spectroscopy analysis

Fig.5 shows the FTIR spectra of MCC and NCC obtained after the cation-exchange resin catalytic hydrolysis. In general, the FTIR spectrum of nanocellulose is very similar to that of MCC. The dominant peaks in the region between 3600 and 2800 cm^{-1} are due to the stretching vibrations of C-H and O-H (Alemdar et al., 2008). The peaks at 3347 cm^{-1} and

2900 cm^{-1} are attributed to the stretching vibrations of O-H and symmetric stretching vibrations of C-H, respectively. The bands in the 1430 cm^{-1} region are due to the C-H deformation vibrations of CH₂ (Ibrahima et al., 2010). The absorbency at 1058 cm^{-1} in the spectrums of MCC and nanocellulose is associated with the C-O stretching vibration. The observation of the peaks at 1112 and 1165 cm^{-1} can be attributed to the C-O and C-C stretching vibration of cellulose ether. And the absorption band at 895 cm^{-1} , for MCC and NCC, respectively, may be regarded as anomeric carbon of cellulose, that is, β -D-glucopyranosyl, which indicates the typical structure of cellulose.

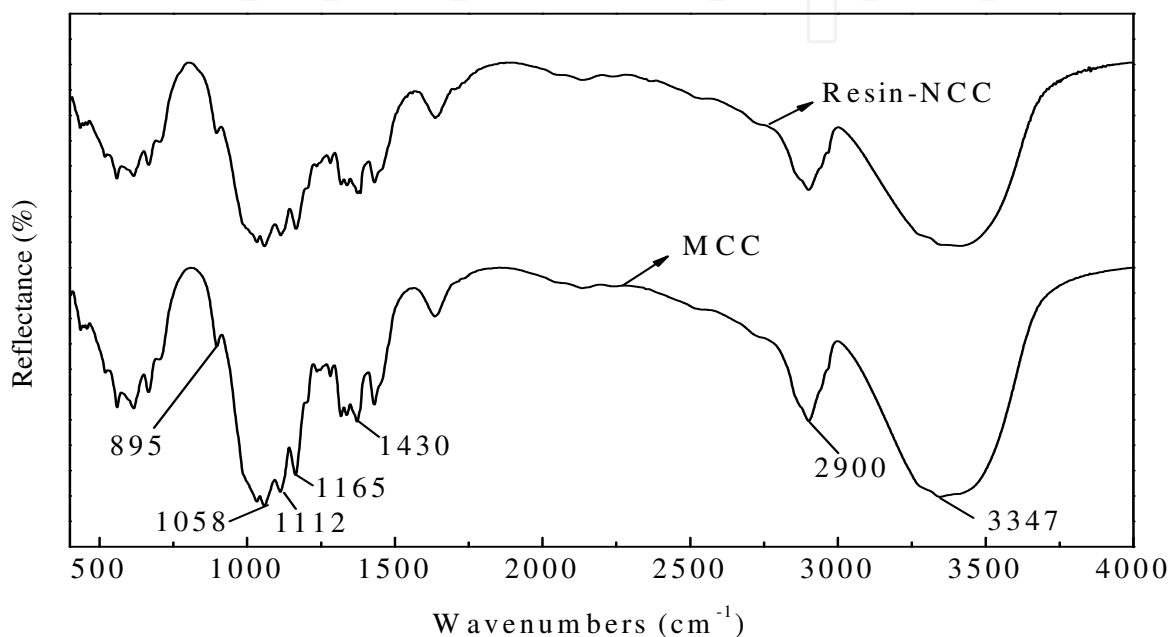


Fig. 5. FTIR spectrum of MCC and NCC.

3.5 Rheological properties of nanocellulose suspension

Fig.6 illustrates the variation of the shear stress of the suspensions with the function of concentration at various shear rates. It shows that the shear stress increases with the rising concentration of NCC. The equilibrium flow curves, τ and $\dot{\gamma}$ (cf. Fig. 7(a)), η and $\dot{\gamma}$ (cf. Fig. 7(b)), of NCC suspensions at various concentrations (2.5%, 3.5%, 4.5%) are shown in Fig.7. All the suspensions display non-Newtonian flow behavior. According to the Ostwald de Waele law, deviation of the flow curve from New-Tonian behavior can be quantified with the flow behavior index, the smaller the value, the greater the degree of shear thinning. The values consistency coefficient and flow behavior for NCC suspension at various concentration are summarized in Table 4. Given a negative value for n , the value for the suspension containing 4.5% NCC is very unusual. This also can be seen from fig. 9a, which shows that shear stress drops when the shear rate increase from 2.0 s^{-1} to 5.0 s^{-1} . It should be noted that this result is quite different from the presented reports. This may be due to the formation of NCC gel. These suspensions exhibit a shear-thinning behaviour, decrease of viscosity with increasing shear rate (cf. Fig. 7(b)).

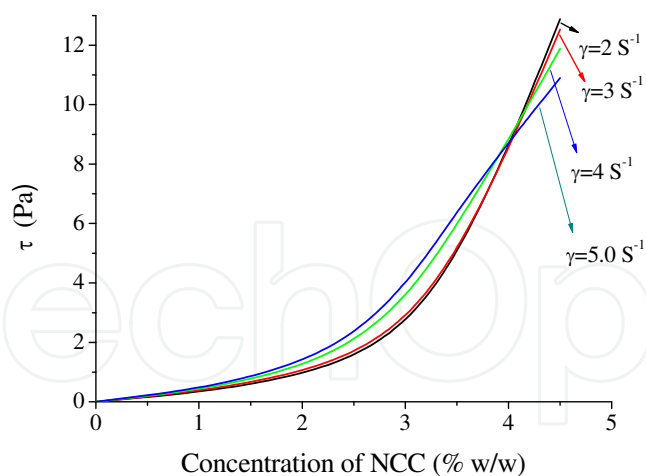


Fig. 6. Variation of the stress with the function of concentration of NCC at various shear rates.

Concentration of NCC Suspension (%)	Flow behavior index, n	Consistency coefficient (Pa s ⁿ)
2.5	-0.199	15.1
3.5	0.478	2.98
4.5	0.273	0.699

Table 4. Power law constants for NCC suspension at various concentrations.

The effect of temperature on the rheological behaviour of the NCC suspensions is also studied. In general, the effect of temperature on rheological properties needs to be documented. Fig 8 shows the effect of temperature on the viscosity of NCC suspensions at various concentrations. The effect of temperature on viscosity of fluid foods at a specified shear rate can be described by the Arrhenius relationship:

$$\eta = Ae^{\frac{E_a}{RT}} \quad (3)$$

where η is the viscosity (Pa s), A is a constant (Pa s), T is the absolute temperature (K), R is the gas constant ($8.315 \text{ J mol}^{-1} \text{ K}^{-1}$), and E_a is the activation energy (J/mol). Generally, the magnitudes of E_a and A can be determined from regression analysis of $1/T$ versus $\ln \eta$. It shows that the viscosity decreases when the temperature increases in the range of $33.5\text{--}68 \text{ }^\circ\text{C}$ for the suspensions at various concentrations. This indicates that the correlation between viscosity and temperature may agree with Arrhenius equation in this range of temperature. The results are summarized in Table 5. As we know, the low E_a values mean that the effect of temperature on the considered parameter is small. The activation energy value (E_a) of NCC suspension will amount to a maximum value when the concentration is 3.5%, which indicates that the decrease in viscosity with temperature rising was more pronounced in this concentration. But after $68 \text{ }^\circ\text{C}$, the relationship between temperature and viscosity displays different curves at various concentrations. The viscosity also

decreases with the increase of temperature for 3.5% NCC suspension, but for 2.5% and 4.5%, the opposite can be observed. This may be due to the swelling of NCC in the water when the temperature increases. It can be observed from Fig.9 that, with temperature rising, the degree of shear thinning is greater.

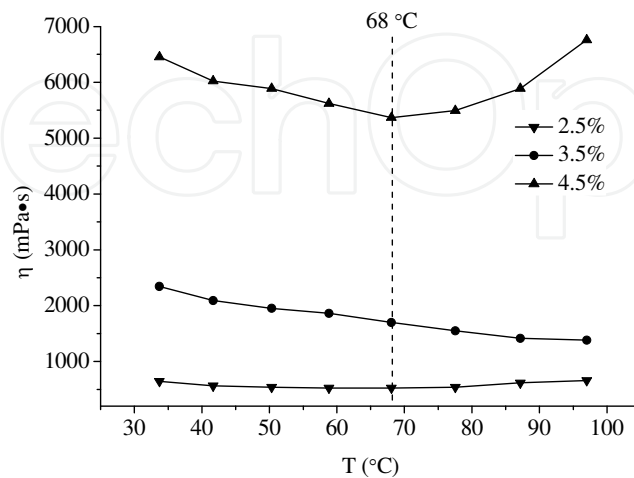


Fig. 8. Variation of the viscosity with a function of the temperature of NCC suspensions at various concentrations.

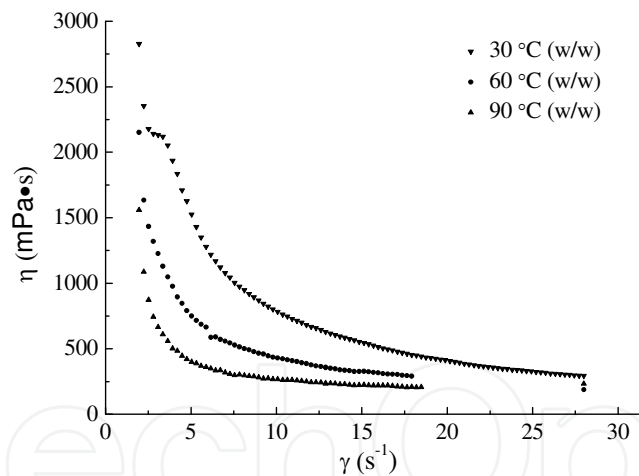


Fig. 9. Variation of the viscosity with a function of shear rate of NCC suspension at various temperatures.

Concentration of NCC (%)	A (Pa s)	Ea (J · mol ⁻¹)	R ²
2.5	0.044	6750	0.88
3.5	0.112	7708	0.90
4.5	1.126	4433	0.98

Table 5. Activation energies (Ea) of NCC suspension at different concentrations (%).

4. Conclusions

NCC is prepared from MCC by cation-exchange resin hydrolysis with the aid of ultrasonification treatment. Compared with liquid acid and alkali chemicals, the main advantages of cation-exchange resin include reduced equipment corrosion, ease of product separation, less potential contamination in waste streams. With RSM and the corresponding Box-Behnken design, the optimal conditions for the production is determined as follows: ratio of NKC-9 to MCC 10: 1, temperature 48 °C, time 189 min. In the optimal conditions, the experiment yield of NCC was 50.04 %, which agrees with the predicted value. NCC prepared by cation-exchange resin hydrolysis presents the interconnected web-like structure, with its diameter mainly in the range of 2-24nm and length in hundreds. The spectrums of FTIR and XRD indicate that the obtained NCC still preserves the basic chemical structure of cellulose. Analyses of the rheological properties of NCC indicate that the suspension is the shear thinned pseudoplastic fluid with solid stability.

5. Acknowledgement

This work was supported by the National Natural Science Foundation of China (Grant NO. 30972312), and Natural Science Foundation of Fujian Province (Grant No. 2010J01270).

6. References

- Alemдар, A. & Sain, M. (2008). Biocomposites from wheat straw nanofibers: Morphology, thermal and mechanical properties, *Composites Science and Technology*, Vol. 68, pp. 557-565.
- Alemдар, A. & Sain M. (2008). Isolation and characterization of nanofibers from agricultural residues – Wheat straw and soy hulls, *Bioresource Technology*, Vol. 99, pp. 1664-1671.
- Aulin, C., Johansson, E., Wågberg, L., et al. (2010). Self-organized films from cellulose I nanofibrils using the layer-by-layer technique, *Biomacromolecules*, Vol. 11, pp. 872-882.
- Cai, Z. J., Y, G. & Kim, J. (2011). Biocompatible nanocomposites prepared by impregnating bacterial cellulose nanofibrils into poly(3-hydroxybutyrate), *Current Applied Physics*, Vol. 11, pp. 247-249.
- Chen, X. P., Wang, W. X., Li, S. B., et al. (2010). Optimization of ultrasound-assisted extraction of Lingzhi polysaccharides using response surface methodology and its inhibitory effect on cervical cancer cells, *Carbohydrate Polymers*, Vol. 80, pp. 944-948.
- de Mesquita, J. P., Donnici, C. L. & Pereira, F. V. (2010). Biobased nanocomposites from layer-by-layer assembly of cellulose nanowhiskers with chitosan, *Biomacromolecules*, Vol. 11, pp. 473-480.
- de Rodriguez, N. L. G., Thielemans, W. & Dufresne, A. (2006). Sisal cellulose whiskers reinforced polyvinyl acetate nanocomposites, *Cellulose*, Vol. 13, pp. 261-270.
- Dufresne, A., Dupeyre, D. & Vignon, M. R. (2000). Cellulose microfibrils from potato tuber cells: Processing and characterization of starch-cellulose microfibril composites, *J. Appl. Polymer Sci*, Vol. 76, pp. 2080-2092.
- Elazzouzi-Hafraoui, S., Nishiyama, Y., Putaux, J. L., et al. (2008). The shape and size distribution of crystalline nanoparticles prepared by acid hydrolysis of native cellulose, *Biomacromolecules*, Vol. 9, No. 1, pp. 57-65.

- Filson, P. B. & Dawson-Andoh, B. E. (2009). Sono-chemical preparation of cellulose nanocrystals from lignocellulose derived materials, *Bioresource Technology*, Vol. 100, No. 7, pp. 2259-2264.
- Fu, J. F., Zhao, Y. Q. & Wu, Q. L. (2007). Optimising photoelectrocatalytic oxidation of fulvic acid using response surface methodology, *Journal of Hazardous Materials*, Vol. 144, pp. 499-505.
- Ghosh, D. & Hallenbeck, P. C. (2010). Response surface methodology for process parameter optimization of hydrogen yield by the metabolically engineered strain *Escherichia coli* DJT135, *Bioresource Technology*, Vol. 101, pp. 1820-1825.
- Harmer, M. A. & Sun, Q. (2001). Solid acid catalysis using ion-exchange resins, *Applied Catalysis A: General*, Vol. 221, pp. 45-62.
- Ibrahima, M. M., Dufresneb A, El-Zawawya, W. K., et al. (2010). Banana fibers and microfibrils as lignocellulosic reinforcements in polymer composites, *Carbohydrate polymers*, Vol. 81, No. 4, pp. 811-819.
- Kaushik, A., Singh, M. & Verma, G. (2010). Green nanocomposites based on thermoplastic starch and steam exploded cellulose nanofibrils from wheat straw, *Carbohydrate Polymers*, Vol. 82, No. 2, pp. 337-345.
- Lee, S. Y., Mohan, D. J., Kang, I. A., et al. (2009). Nanocellulose Reinforced PVA Composite Films: Effects of Acid Treatment and Filler Loading, *Fibers and Polymers*, Vol. 10, No. 1, pp. 77-82.
- Majumder, A., Singh, A. & Goyal, A. (2009). Application of response surface methodology for glucan production from *Leuconostoc dextranicum* and its structural characterization, *Carbohydrate Polymers*, Vol. 75, pp. 150-156.
- Medeiros, E. S., Mattoso, L. H., Bernardes-Fiho, R., et al. (2008). Self-assembled films of cellulose nanofibrils and poly(*o*-ethoxyaniline), *Colloid Polymer Science*, Vol. 286, pp. 1265-1272.
- Mendez, J. D. & Weder, C. (2010). Synthesis, electrical properties, and nanocomposites of poly(3,4-ethylenedioxythiophene) nanorods, *Polymer Chemistry*, Vol. 1, No. 8, pp. 1237-1244.
- Morán, J. I., Alvarez, V. A., Cyras, V. P., et al. Extraction of cellulose and preparation of nanocellulose from sisal fibers, *Cellulose*, 2008, Vol. 15, No. 1, pp. 149-159.
- Nogi, M., Iwamoto, S., Nakagaito, A. N., et al. (2009). Optically Transparent Nanofiber Paper, *Advanced materials*, Vol. 21, No. 16, pp. 1595-1598.
- Pääkko, M., Ankerfors, M., Kosonen, H., et al. (2007). Enzymatic hydrolysis combined with mechanical shearing and high-pressure homogenization for nanoscale cellulose fibrils and strong gels, *Biomacromolecules*, Vol. 8, No. 6, pp. 1934-1941.
- Panthapulakkal, S., Zereshkian, A. & Sain, M. (2006). Preparation and characterization of wheat straw fibers for reinforcing application in injection molded thermoplastic composites, *Bioresource Technology*, Vol. 97, pp. 265-272.
- Pei, A., Zhou, Q. & Berglund, L. A. (2010). Functionalized cellulose nanocrystals as biobased nucleation agents in poly(L-lactide) (PLLA) - crystallization and mechanical property effects, *Composites Science and Technology*, Vol. 70, pp. 815-821.
- Siró, I. & Plackett, D. (2001). Microfibrillated cellulose and new nanocomposite materials: a review, *Cellulose*, Vol. 17, No. 3, pp. 459-494.

- Tingaut, P., Zimmermann, T. & Lopez-Suevos, F. (2010). Synthesis and characterization of bionanocomposites with tunable properties from poly(lactic acid) and acetylated microfibrillated cellulose, *Biomacromolecules*, Vol. 11, No. 2, pp. 454-464.
- Tischer, P. C. S. F., Sierakowski, M. R., Westfahl, H., et al. (2010). Nanostructural reorganization of bacterial cellulose by ultrasonic treatment, *Biomacromolecules*, Vol. 11, No. 5, pp. 1217-1224.
- Wang, S. & Cheng, Q. (2009). A Novel Process to isolate fibrils from cellulose fibers by high-intensity ultrasonication, *Journal of applied polymer science*, Vol. 113, No. 2, pp. 1270-1275.
- Wang, Y. X., Tian, H. F. & Zhang, L. N. (2010). Role of starch nanocrystals and cellulose whiskers in synergistic reinforcement of waterborne polyurethane, *Carbohydrate Polymers*, Vol. 80, pp. 665-671.
- Wikipedia. (2011). Nanocellulose, In: *Wikipedia*, accessed on 24 April 2011, Available from: <http://en.wikipedia.org/wiki/Nanocellulose>.
- Zhao, H. P. & Feng, X. Q. (2007). Ultrasonic technique for extracting nanofibers from nature materials, *Applied physics letters*, Vol. 90, No. 7, 073112 (1-2).
- Zimmermann, T., Bordeanu, N. & Strub E. (2010). Properties of nanofibrillated cellulose from different raw materials and its reinforcement potential, *Carbohydrate Polymers*, Vol. 79, pp. 1086-1093.
- Zuluaga, R., Putaux, J. L., Cruz, J., et al. (2009). Cellulose microfibrils from banana rachis: Effect of alkaline treatments on structural and morphological features, *Carbohydrate Polymers*, Vol. 76, No. 1, pp. 51-59.

IntechOpen



Biomaterials Science and Engineering

Edited by Prof. Rosario Pignatello

ISBN 978-953-307-609-6

Hard cover, 456 pages

Publisher InTech

Published online 15, September, 2011

Published in print edition September, 2011

These contribution books collect reviews and original articles from eminent experts working in the interdisciplinary arena of biomaterial development and use. From their direct and recent experience, the readers can achieve a wide vision on the new and ongoing potentials of different synthetic and engineered biomaterials. Contributions were not selected based on a direct market or clinical interest, than on results coming from very fundamental studies which have been mainly gathered for this book. This fact will also allow to gain a more general view of what and how the various biomaterials can do and work for, along with the methodologies necessary to design, develop and characterize them, without the restrictions necessarily imposed by industrial or profit concerns. The book collects 22 chapters related to recent researches on new materials, particularly dealing with their potential and different applications in biomedicine and clinics: from tissue engineering to polymeric scaffolds, from bone mimetic products to prostheses, up to strategies to manage their interaction with living cells.

How to reference

In order to correctly reference this scholarly work, feel free to copy and paste the following:

Huang Biao, Tang Li-rong, Dai Da-song, Ou Wen, Li Tao and Chen Xue-rong (2011). Preparation of Nanocellulose with Cation–Exchange Resin Catalysed Hydrolysis, *Biomaterials Science and Engineering*, Prof. Rosario Pignatello (Ed.), ISBN: 978-953-307-609-6, InTech, Available from:
<http://www.intechopen.com/books/biomaterials-science-and-engineering/preparation-of-nanocellulose-with-cation-exchange-resin-catalysed-hydrolysis>

INTECH
open science | open minds

InTech Europe

University Campus STeP Ri
Slavka Krautzeka 83/A
51000 Rijeka, Croatia
Phone: +385 (51) 770 447
Fax: +385 (51) 686 166
www.intechopen.com

InTech China

Unit 405, Office Block, Hotel Equatorial Shanghai
No.65, Yan An Road (West), Shanghai, 200040, China
中国上海市延安西路65号上海国际贵都大饭店办公楼405单元
Phone: +86-21-62489820
Fax: +86-21-62489821

© 2011 The Author(s). Licensee IntechOpen. This chapter is distributed under the terms of the [Creative Commons Attribution-NonCommercial-ShareAlike-3.0 License](#), which permits use, distribution and reproduction for non-commercial purposes, provided the original is properly cited and derivative works building on this content are distributed under the same license.

IntechOpen

IntechOpen